ChemComm

COMMUNICATION

View Article Online
View Journal | View Issue

Cite this: *Chem. Commun.*, 2020, **56**, 3289

Received 20th December 2019,
Accepted 5th February 2020

DOI: 10.1039/c9cc09865h

rsc.li/chemcomm

Novel small-molecule fluorophores for *in vivo* NIR-IIa and NIR-IIb imaging†

Qianqian Li,‡[ab] Qihang Ding,‡[a] Yang Li,[a] Xiaodong Zeng,[a] Yishen Liu,[a] Siyu Lu,[a] Hui Zhou,[a] Xiaofei Wang,[c] Junzhu Wu,[c] Xianli Meng,[d] Zixin Deng[a] and Yuling Xiao *[ab]

Near-infrared fluorescence imaging in the 1000–1700 nm-wavelength window (NIR-II) has exhibited great potential for deep-tissue bioimaging due to its diminished auto-fluorescence, suppressed photo-scattering, deep penetration, and high spatial and temporal resolutions. Various kinds of inorganic nanomaterials have been extensively developed for NIR-IIa (1300–1400 nm) and NIR-IIb (1500–1700 nm) bioimaging. However, the development of small-molecule NIR-IIa and NIR-IIb fluorophores is still in its infancy. Herein, we designed and synthesized a novel NIR-II organic aggregation-induced emission (AIE) fluorophore (HQL2) with a fluorescence tail extending into the NIR-IIa and NIR-IIb region based on our previous reported skeleton Q4. The encapsulated NIR-II AIE nanoparticles (HQL2 dots) exhibited water solubility and biocompatibility, and high brightness for NIR-IIa and NIR-IIb vascular imaging *in vivo*, a first for NIR-II AIE dots.

Vascular diseases such as cardiocerebrovascular diseases and stroke are considered to be "top killers" and seriously affect the quality of life of people. Assessment of vascularity is crucial for achieving a precise diagnosis and treatment of such diseases. Up to now, various kinds of imaging techniques such as magnetic resonance imaging (MRI),[1] Doppler ultrasonography,[2] positron emission tomography (PET)[3] and X-ray computer tomography (CT)[4] have been widely used in clinical research. Recently, fluorescence imaging in the second near-infrared region (NIR-II, 1000–1700 nm) has been considered as a potential imaging technique, and has been widely studied for vascular imaging and tumor diagnosis due to its minimum light scattering, reduced auto-fluorescence and high penetration depth.[5–12] Various inorganic and organic NIR-II materials, with maximum emission wavelengths below 1300 nm, have been developed for biomedical applications.[13–30] Furthermore, molecular optical imaging in the NIR-IIa (1300–1400 nm) and NIR-IIb (1500–1700 nm) sub-windows displays nearly zero auto-fluorescence and a super resolution.[31–35] So far, very few small-molecule NIR-IIa and NIR-IIb fluorophores for fluorescence imaging in the long-wavelength region have been reported.[23,29–37] Of note, the organic dye **FD-1080** was first employed for NIR-IIb vascular imaging with J-aggregates and showed a quantum yield of 0.0545%.[37] Thus, developing a variety of small-molecule fluorophores having emission wavelenghts beyond 1300 and 1500 nm with high *in vivo* imaging quality and negligible background signals is indispensable. A potential way to develop such fluorophores is to make comprehensive use of the bright highly twisted NIR-II emitters with strong emission extending into the NIR-IIb region by following the aggregation-induced emission (AIE) strategy.[38,39]

Herein, the previously reported NIR-II molecule **Q4**[40] was modified by introducing dodecyl side chains into the different positions of the electron-rich thiophene spacer. Two highly twisted NIR-II dyes, **HQL1** and **HQL2**, were obtained. Surprisingly, **HQL2** showed high brightness and high quantum yield with AIE characteristics. Its maximum emission wavelength was ~1050 nm, and the emission extended to 1600 nm. Then, **HQL2** dots were prepared by encapsulating **HQL2** with the amphiphilic molecule **DSPE-PEG5K**. The encapsulated NIR-II AIE **HQL2** dots exhibited excellent photostability and biocompatibility, and were used for *in vivo* NIR-IIa and NIR-IIb vascular imaging. To the best of our knowledge, this is the first time that NIR-II AIE dots have been exploited in the NIR-IIa and NIR-IIb region for *in vivo* imaging.

As illustrated in Fig. 1A, the fluorophores **HQL1** and **HQL2** employed a D–A–D structure with benzo-bis(1,2,5-thiadiazole (BBTD) as the acceptor, and a thiophene ring and Ph_3N as the donor units. To minimize energy transfer and reduce intermolecular interactions between the fluorophores and the surrounding

[a] *State Key Laboratory of Virology, Key Laboratory of Combinatorial Biosynthesis and Drug Discovery (MOE), Hubei Province Engineering and Technology Research Center for Fluorinated Pharmaceuticals, Wuhan University School of Pharmaceutical Sciences, Wuhan 430071, China. E-mail: xiaoyl@whu.edu.cn*
[b] *College of Science, Innovation Center for Traditional Tibetan Medicine Modernization and Quality Control, Medical College, Tibet University, Lasa, 850000, China*
[c] *Hubei Provincial Key Laboratory of Developmentally Originated Disease, Center for Experimental Basic Medical Education, Wuhan 430071, China*
[d] *Innovative Institute of Chinese Medicine and Pharmacy, Chengdu University of Traditional Chinese Medicine, Chengdu, Sichuan 611137, China*

† Electronic supplementary information (ESI) available. See DOI: 10.1039/c9cc09865h

‡ These authors contributed equally to this work.

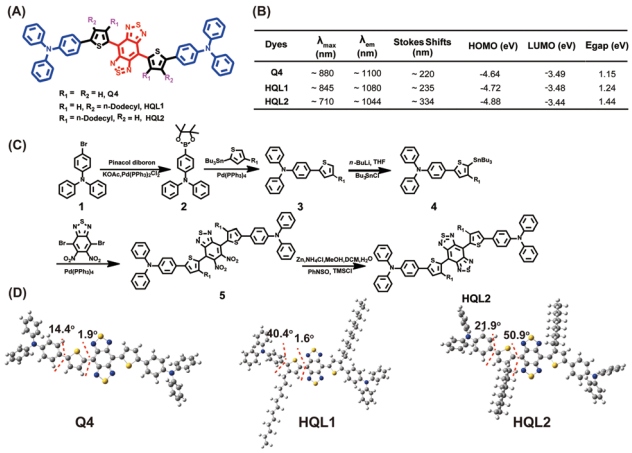

Dyes	λ_{max} (nm)	λ_{em} (nm)	Stokes Shifts (nm)	HOMO (eV)	LUMO (eV)	Egap (eV)
Q4	~ 880	~ 1100	~ 220	-4.64	-3.49	1.15
HQL1	~ 845	~ 1080	~ 235	-4.72	-3.48	1.24
HQL2	~ 710	~ 1044	~ 334	-4.88	-3.44	1.44

Fig. 1 (A) Design of NIR-IIa and IIb dyes based on AIE and a highly twisted structure, specifically showing the chemical structures of **Q4**, **HQL1** and **HQL2**. (B) Optical property measures and the results of molecular orbital calculations for **Q4**, **HQL1** and **HQL2**. (C) The synthetic route to **HQL2**. (D) Calculated optimized ground state (S_0) geometries of the molecules at the B3LYP/6-31G(d,p) level.

water, the hydrophobic alkyl group was integrated at the position R_1 or R_2. **HQL1** and **HQL2** were feasibly synthesized from **Q4** according to the modified procedure (Fig. 1B and ESI†). Generally, the donor unit Ph_3N conjugates to the thiophene unit first, and then couples to the acceptor BBTD to yield the desired products, mainly through Suzuki–Miyaura coupling, Stille coupling, Zn/NH_4Cl reduction and *N*-thionylaniline-induced ring closure in 42–48.6% overall yields from the starting materials. All compounds were characterized using ^{1}H-NMR, ^{13}C-NMR and MALDI-TOF-MS or ESI-MS (Fig. S1–S14, ESI†), and showed excellent levels of solubility in various organic solvents.

The highest occupied molecular orbitals (HOMOs), lowest unoccupied molecular orbitals (LUMOs) and energy gaps (E_{gaps}) of these molecules calculated using Gaussian 09 software with 6-31G(d,p) basis sets revealed the importance of the dodecyl side chains at the different positions of thiophene. The substitution had strong effects on the molecular orbitals and molecular distortion. Positioning the dodecyl side chain close to the BBTD core increased the LUMO energy level and decreased that of the HOMO. All molecules showed optical bandgaps lower than 1.5 eV, which was regarded as one of the thresholds for NIR-II BBTD dyes. Upon photoexcitation of the S_0 state, the molecular twist angle of **HQL2** (50.9°) was much larger than those of **HQL1** (1.6°) and **Q4** (1.9°), revealing an order of distortion following the trend R_1 = dodecyl, R_2 = H > R_1 = R_2 = H > R_1 = H, R_2 = dodecyl between the thiophene donor and BBTD core (Fig. 1D and Fig. S15, ESI†). Various optical properties of HQL1 and HQL2 were also evaluated. HQL1 and HQL2 in dichloromethane (DCM) showed maximum emission wavelengths of ~1080 nm and ~1044 nm with emission QYs of 0.699% and 0.149%, respectively (Fig. S18 and S19, ESI†). Introduction of the molecular distortion at the R_1 position caused a remarkable increase in fluorescence intensity with a 20–50 nm wavelength hypsochromic shift compared with **Q4** (Fig. 1B and 2A). To determine the mechanism behind this phenomenon, the optical properties of **HQL1** and **HQL2** in various THF-water mixtures with different relative amounts of THF and water were investigated. The fluorescence intensity of **HQL1** decreased as the relative amount of water was increased, indicative of obvious aggregation-caused quenching (ACQ) effects (Fig. S16, ESI†). In contrast, **HQL2** showed a significant AIE effect (Fig. 2B and C). As shown in Fig. 2D, a strong fluorescence of **HQL2** in a water/THF mixture (9 : 1 v/v) was observed in comparison with that of **HQL2** in pure THF. The molar absorption coefficients of **HQL1** and **HQL2** in DCM were determined to be 2.14×10^5 L mol^{-1} cm^{-1} and 1.98×10^4 L mol^{-1} cm^{-1}, respectively. Based on these results, a tentative mechanism was proposed. According to this proposed mechanism, the inclusion of **HQL2** resulted in a very strong fluorescence enhancement in the NIR-IIa and NIR-IIb windows, with its highly twisted backbone (*i.e.*, having high dihedral angles) having reduced the intramolecular charge transfer (ICT)-induced fluorescence quenching effects, and increased the AIE-induced fluorescence enhancement effects using triphenylamine as a building block of AIEgens. These interesting results indicate that the novel light-up fluorophore **HQL2** is suitable for *in vivo* NIR-IIa and NIR-IIb imaging.

HQL2 was then encapsulated in **DSPE-PEG5K** to form **HQL2** dots according to the literature method.[23] These dots have spherical shapes with an average particle size of ~125.9 nm and hydrodynamic size of ~155 nm, as determined from transmission electron microscopy (TEM) and dynamic light scattering (DLS) analyses, respectively (Fig. S21A and B, ESI†). The zeta potential of the **HQL2** dots in PBS was determined to be −24.1 eV (Fig. S17, ESI†). The UV-Vis-NIR spectra of the **HQL2** dots demonstrated peak absorption and emission wavelengths similar to those of **HQL2**, and tails into the 1600 nm wavelength region (Fig. S21C, ESI†).

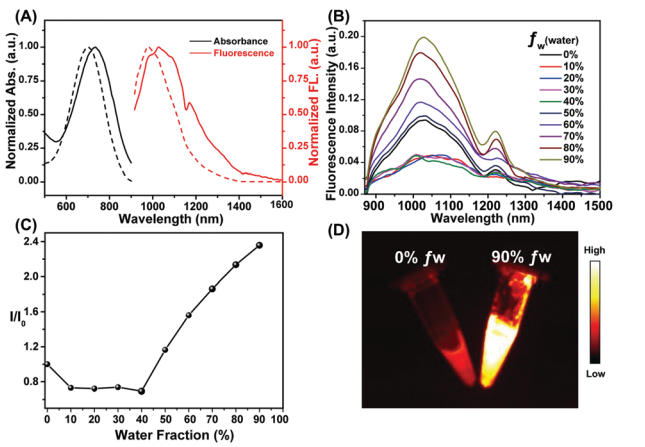

Fig. 2 (A) The acquired UV-Vis-NIR absorption spectra (black) and NIR-II fluorescence spectra (red) of **HQL1** (bold line) and **HQL2** (dash line) in DCM. (B) The acquired fluorescence spectra of **HQL2** in various THF/water mixtures with different water fraction (f_w) values. (C) The fluorescence intensity ratio (I/I_0) values of **HQL2** in the various mixtures with different values of f_w, based on the integrated fluorescence intensities shown in panel B, and with I_0 being the fluorescence intensity of **HQL2** in pure THF with 808 nm-wavelength excitation (5 ms exposure time, 90 mW cm^{-2}). (D) NIR II image of **HQL2** in pure THF (left) and in a water/THF mixture (9 : 1 v/v, right) with 808 nm excitation (5 ms exposure time, 1000 nm LP, 90 mW cm^{-2}).

The molar absorption coefficient of HQL2 in water was measured to be $\sim 5.44 \times 10^4$ L mol^{-1} cm^{-1}, 5-fold larger than that of HQL1 (ε: $\sim 1.06 \times 10^4$ L mol^{-1} cm^{-1}) in water, demonstrating the greater brightness of HQL2 and its superiority for imaging. The fluorescence of the **HQL2** dots (100 μg mL^{-1}) could even be detected using a 1320 nm-wavelength long-pass (LP) filter and 1550 nm wavelength LP filter under an 808 nm wavelength excitation with extended exposure time (Fig. S21D, ESI†). The QY of the **HQL2** dots was determined to be 1.19% in the NIR-II region (>1000 nm) in water with IR-26 (QY: 0.05%) as a reference, and 0.016% beyond 1300 nm, and 0.002% beyond 1550 nm (Fig. S18, ESI†).[18,26] The **HQL2** dots showed negligible decay in phosphate-buffered saline (PBS), fetal bovine serum (FBS) and water under 808 nm laser excitation for 60 min (180 mW cm^{-2}, 10 ms exposure time) (Fig. S21E, ESI†), revealing the excellent photostability of these dots. The *in vitro* cell cytotoxicity of the **HQL2** dots was studied in human hepatocyte L02 cell lines using the standard 3-(4,5-dimethylthiazol-2-yl)-2,5-diphenyl tetrazolium bromide (MTT) assay. As shown in Fig. S21F (ESI†), the cell viability of the L02 cells was much higher than ~80% when incubated for 24 h even with a high concentration of **HQL2** (80 μg mL^{-1}). The blood circulation half-life was ~226.5 min, determined by a quantification of the fluorescence intensity of **HQL2** dots in the bloodstreams of female KM mice (n = 3) (Fig. S20, ESI†). These results showed a low cytotoxicity and good biocompatibility of the **HQL2** dots, indicating the great potential of using these dots for *in vivo* NIR-IIa and NIR-IIb imaging.

Real-time monitoring the dynamic change of blood vessels in the areas of lesions is of great significance for the diagnosis and treatment of cancer. *In vivo* NIR-IIa and NIR-IIb vascular imaging analyses were conducted by performing an intravenous injection of a sample of the **HQL2** dots (200 μL, 5 mg mL^{-1}) into C57 Balb/c (n = 3 per group) (Fig. 3A). The whole angiography was visualized using an InGaAs camera with different LP filters (1000, 1250, 1320 and 1550 nm) under 808 nm wavelength laser excitation (90 mW cm^{-2}). The imaging of the **HQL2** dots in the NIR-IIa window (1300–1400 nm, 1320 nm LP) with a 200 ms exposure time yielded superior resolution (Fig. 3A). An extended exposure time (800 ms) was required for high-resolution NIR-IIb imaging. The signal-to-background ratio (S/B) of the NIR-IIa imaging (S/B = 2.5, 1320 nm LP) was 2.5-fold higher than that of the NIR-II imaging (S/B = 1, 1000 nm LP and 1250 nm LP), and was also 1.4-fold higher than that of the NIR-IIb imaging (S/B = 1.8, 1550 nm LP) due to the low quantum yield beyond 1550 nm. The Gaussian-fitted full width at half maximum (FWHM) values of the vessels at the same position (in red dashed line) under different long-pass filters were calculated to be 2.13 mm (1000 nm LP), 1.05 mm (1250 nm LP), 0.345 mm (1320 nm LP) and 0.529 mm (1550 nm LP), respectively (Fig. 3B), demonstrating the great potential of using **HQL2** dots for *in vivo* NIR-IIa and NIR-IIb imaging at extended exposure times.

Tumor angiogenesis can provide specific information for clinical research such as tumorigenesis and metastasis, and plays a crucial role in cancer diagnosis and treatment. For *in vivo* NIR-IIa and NIR-IIb tumor vessel imaging, samples of **HQL2** dots (200 μL, 5 mg mL^{-1}) were administered to U87MG-tumor-bearing female Balb/c nude mice (n = 3) through a tail vein injection. The tumor vascular imaging was performed immediately thereafter under an 808 nm laser excitation with various long-pass (LP) filters. The tumor vessels (red dashed line in Fig. 4C and D) were imaged clearly using the 1320 nm LP (NIR-IIa) and 1550 nm LP (NIR-IIb). The FWHM values of the tiny vessels (red dashed lines in Fig. 4C and D) were measured to be 0.293 mm (1320 nm LP) and 0.124 mm (1550 nm LP), respectively (Fig. 4E and F).

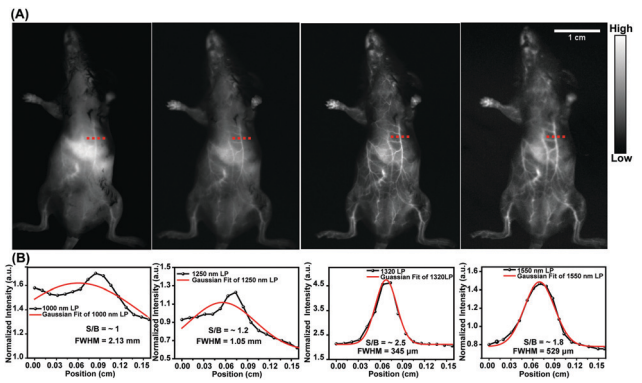

Fig. 3 (A) The acquired fluorescence images of whole vessels in the abdomens of C57 Balb/c female mice using samples of the **HQL2** dots under 808 nm-wavelength laser excitation (90 mW cm^{-2}) with different long-pass filters (left to right: 1000, 1250, 1320, 1550 nm). (B) Cross-section intensity (black line) and Gaussian fit fluorescence intensity (red line) profiles with **HQL2** dot imaging of the tiny vessels in Fig. 3A (red dashed line).

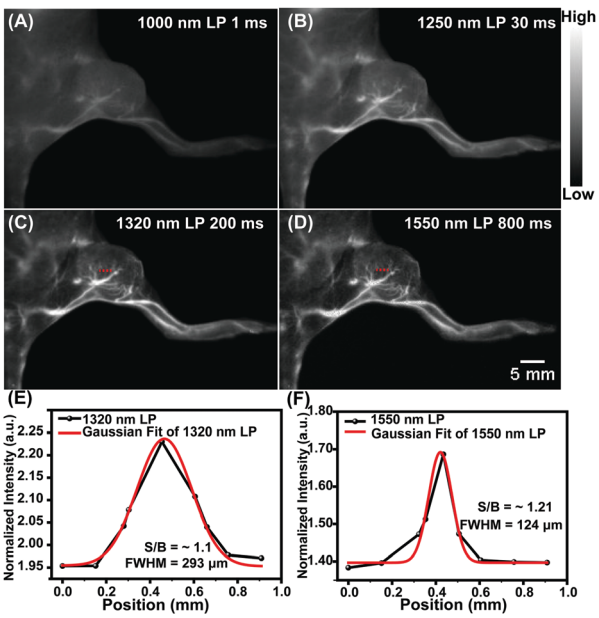

Fig. 4 (A–D) The acquired fluorescence images of U87MG-tumor-bearing nude mice with different filters and exposure times under 808 nm-wavelength excitation (90 mW cm^{-2}): (A) 1000 nm LP, 1 ms; (B) 1250 nm LP, 30 ms; (C) 1320 nm, 200 ms; and (D) 1550 nm LP, 800 ms. (E and F) Cross-section intensity (black line) and Gaussian fit fluorescence intensity (red line) profiles of tiny vessels (red dashed lines in figure C and D) with **HQL2** dot imaging using different long-pass filters, namely (E) the 1320 nm LP and (F) the 1550 nm LP.

In contrast, no desired tiny tumor vessels were detected using 1000 nm LP and 1250 nm LP owing to the relatively low resolution (Fig. 4A and B).

In summary, two novel NIR-II dyes, **HQL1** and **HQL2** based on our previous reported molecule **Q4**, were designed and synthesized. Inclusion of **HQL2** with its large donor–acceptor distortion and strong NIR-II AIE yielded a remarkable increase in NIR-II fluorescence intensity. **HQL2** dots encapsulated with **DSPE-PEG5K** showed strong fluorescence intensity beyond 1300 nm and 1550 nm with excellent photostability and biocompatibility, and were applied for *in vivo* NIR-IIa and NIR-IIb vascular and tumor vessel imaging under 808 nm-wavelength excitation. As far as we are concerned, the development of small-molecule fluorophores for bioimaging beyond 1300 nm and 1550 nm is still in its infancy. This novel NIR-II fluorophore **HQL2** may nevertheless open up new approaches for the rational design of novel small molecules for NIR-IIa and NIR-IIb imaging with deep penetration and high resolution.

This work was partially supported by grants from the NSFC (81773674, 21473041, 81573383), the Project First-Class Disciplines Development Supported by Chengdu University of Traditional Chinese Medicine (CZYJC1903), the NSFHP (2017CFA0 24, 2016ACA126, 2017CFB711), the Tibet Autonomous Region Science and Technology Plan Project Key Project (XZ201901-GB-11), the Applied Basic Research Program of WMBST (2019020701011429), the Fundamental Research Funds for the Central Universities, and the Health Commission of Hubei Province Scientific Research Project (WJ2019M178, WJ2019M177).

Conflicts of interest

There are no conflicts to declare.

Notes and references

1 C. Jacoby, Y. C. Böring, A. Beck, A. Zernecke, V. Aurich, C. Weber, J. Schrader and U. Flögel, *J. Magn. Reson. Imaging*, 2008, **28**, 637–645.
2 J. W. Wladimiroff, H. M. Tonge and P. A. Stewart, *BJOG*, 1986, **93**, 471–475.
3 W. Chen and V. Dilsizian, *J. Nucl. Med.*, 2015, **56**, 503–504.
4 S. Kunjachan, J. Ehling, G. Storm, F. Kiessling and T. Lammers, *Chem. Rev.*, 2015, **115**, 10907–10937.
5 G. Hong, J. C. Lee, J. T. Robinson, U. Raaz, L. Xie, N. F. Huang, J. P. Cooke and H. Dai, *Nat. Med.*, 2012, **18**, 1841–1846.
6 C. Qu, Y. Xiao, H. Zhou, B. Ding, A. Li, J. Lin, X. Zeng, H. Chen, K. Qian, X. Zhang, W. Fang, J. Wu, Z. Deng, Z. Cheng and X. Hong, *Adv. Opt. Mater.*, 2019, **7**, 1900229.
7 G. Hong, A. L. Antaris and H. Dai, *Nat. Biomed. Eng.*, 2017, **1**, 0010.
8 G. Hong, J. T. Robinson, Y. Zhang, S. Diao, A. L. Antaris, Q. Wang and H. Dai, *Angew. Chem., Int. Ed.*, 2012, **51**, 9818.
9 C. Li, Y. Zhang, M. Wang, Y. Zhang, G. Chen, L. Li, D. Wu and Q. Wang, *Biomaterials*, 2014, **35**, 393–400.
10 Y. Du, B. Xu, T. Fu, M. Cai, F. Li, Y. Zhang and Q. Wang, *J. Am. Chem. Soc.*, 2010, **132**, 1470–1471.
11 Y. Tang, F. Pei, X. Lu, Q. Fan and W. Huang, *Adv. Opt. Mater.*, 2019, **7**, 1900917.
12 Q. Wang, Y. Dai, J. Xu, J. Cai, X. Niu, L. Zhang, R. Chen, Q. Shen, W. Huang and Q. Fan, *Adv. Funct. Mater.*, 2019, **29**, 1901480.
13 J. T. Robinson, G. Hong, Y. Liang, B. Zhang, O. K. Yaghi and H. Dai, *J. Am. Chem. Soc.*, 2012, **25**, 10664–10669.
14 R. Wang, X. Li, L. Zhou and F. Zhang, *Angew. Chem., Int. Ed.*, 2014, **53**, 12086–12090.
15 J.-Y. Zhao, G. Chen, Y.-P. Gu, R. Cui, Z.-L. Zhang, Z.-L. Yu, B. Tang, Y.-F. Zhao and D.-W. Pang, *J. Am. Chem. Soc.*, 2016, **138**, 1893–1903.
16 S. He, J. Song, J. Qu and Z. Cheng, *Chem. Soc. Rev.*, 2018, **47**, 4258–4278.
17 Z. Liu, F. Ren, H. Zhang, Q. Yuan, Z. Jiang, H. Liu, Q. Sun and Z. Li, *Biomaterials*, 2019, **219**, 119364.
18 A. L. Antaris, H. Chen, K. Cheng, Y. Sun, G. Hong, C. Qu, S. Diao, Z. Deng, X. Hu, B. Zhang, X. Zhang, O. K. Yaghi, Z. R. Alamparambil, X. Hong, Z. Cheng and H. Dai, *Nat. Mater.*, 2016, **15**, 235–242.
19 J. Yang, Q. Xie, H. Zhou, L. Chang, W. Wei, Y. Wang, H. Li, Z. Deng, Y. Xiao, J. Wu, P. Xu and X. Hong, *J. Proteome Res.*, 2018, **17**, 2428–2439.
20 H. Zhou, H. Yang, L. Tang, Y. Wang, Y. Li, N. Liu, X. Zeng, Y. Yan, J. Wu, S. Chen, L. Xiao, Y. Yu, Z. Deng, H. Deng, X. Hong and Y. Xiao, *J. Mater. Chem. C*, 2019, **7**, 9448–9454.
21 X. Zeng, Y. Xiao, J. Lin, S. Li, H. Zhou, J. Nong, G. Xu, H. Wang, F. Xu, J. Wu, Z. Deng and X. Hong, *Adv. Healthcare Mater.*, 2018, **7**, 1800589.
22 R. Tian, H. Ma, Q. Yang, H. Wan, S. Zhu, S. Chandra, H. Sun, D. O. Kiesewetter, G. Niu, Y. Liang and X. Chen, *Chem. Sci.*, 2019, **10**, 326–332.
23 J. Lin, X. Zeng, Y. Xiao, L. Tang, J. Nong, Y. Liu, H. Zhou, B. Ding, F. Xu, H. Tong, Z. Deng and X. Hong, *Chem. Sci.*, 2019, **10**, 1219–1226.
24 X. Zeng, L. Xue, D. Chen, S. Li, J. Nong, B. Wang, L. Tang, Q. Li, Y. Li, Z. Deng, X. Hong, M. Wu and Y. Xiao, *Chem. Commun.*, 2019, **55**, 14287–14290.
25 Z. Sheng, B. Guo, D. Hu, S. Xu, W. Wu, W. H. Liew, K. Yao, J. Jiang, C. Liu, H. Zheng and B. Liu, *Adv. Mater.*, 2018, **30**, 1800766.
26 F. Ren, L. Ding, H. Liu, Q. Huang, H. Zhang, L. Zhang, J. Zeng, Q. Sun, Z. Li and M. Gao, *Biomaterials*, 2018, **175**, 30–43.
27 Y. Xu, F. Ren, H. Liu, H. Zhang, Y. Han, Z. Liu, W. Wang, Q. Sun, C. Zhao and Z. Li, *ACS Appl. Mater. Interfaces*, 2019, **11**, 21399–21407.
28 B. Ding, Y. Xiao, H. Zhou, X. Zhang, C. Qu, F. Xu, Z. Deng, Z. Cheng and X. Hong, *J. Med. Chem.*, 2019, **62**, 2049–2059.
29 X. Zeng, Z. Chen, L. Tang, H. Yang, N. Liu, H. Zhou, Y. Li, J. Wu, Z. Deng, Y. Yu, H. Deng, X. Hong and Y. Xiao, *Chem. Commun.*, 2019, **55**, 2541–2544.
30 S. Wang, Y. Fan, D. Li, C. Sun, Z. Lei, L. Lu, T. Wang and F. Zhang, *Nat. Commun.*, 2019, **10**, 1058.
31 Z. Zhang, X. Fang, Z. Liu, H. Liu, D. Chen, S. He, J. Zheng, B. Yang, W. Qin, X. Zhang and C. Wu, *Angew. Chem., Int. Ed.*, 2019, DOI: 10.1002/anie.201914397.
32 Z. Xue, S. Zeng and J. Hao, *Biomaterials*, 2018, **171**, 153–163.
33 S. Wang, L. Liu, Y. Fan, A. M. El-Toni, M. S. Alhoshan, D. Li and F. Zhang, *Nano Lett.*, 2019, **19**, 2418–2427.
34 Z. Deng, X. Li, Z. Xue, M. Jiang, Y. Li, S. Zeng and H. Liu, *Nanoscale*, 2018, **10**, 9393–9400.
35 Y. Li, S. Zeng and J. Hao, *ACS Nano*, 2019, **13**, 248–259.
36 Y. Zhong, Z. Ma, S. Zhu, J. Yue, M. Zhang, A. L. Antaris, J. Yuan, R. Cui, H. Wan, Y. Zhou, W. Wang, N. F. Huang, J. Luo, Z. Hu and H. Dai, *Nat. Commun.*, 2017, **8**, 737.
37 C. Sun, B. Li, M. Zhao, S. Wang, Z. Lei, L. Lu, H. Zhang, L. Feng, C. Dou, D. Yin, H. Xu, Y. Cheng and F. Zhang, *J. Am. Chem. Soc.*, 2019, **141**, 19221–19225.
38 S. Liu, X. Zhou, H. Zhang, H. Ou, J. W. Y. Lam, Y. Liu, L. Shi, D. Ding and B. Z. Tang, *J. Am. Chem. Soc.*, 2019, **141**, 5359–5368.
39 Q. Yang, Z. Hu, S. Zhu, R. Ma, H. Ma, Z. Ma, H. Wan, T. Zhu, Z. Jiang, W. Liu, L. Jiao, H. Sun, Y. Liang and H. Dai, *J. Am. Chem. Soc.*, 2018, **140**, 1715–1724.
40 Y. Sun, C. Qu, H. Chen, M. He, C. Tang, K. Shou, S. Hong, M. Yang, Y. Jiang, B. Ding, Y. Xiao, L. Xing, X. Hong and Z. Cheng, *Chem. Sci.*, 2016, **9**, 6203–6207.

